



Ursolic acid induces apoptosis and pyroptosis in Reh cells by upregulating of the JNK signalling pathway based on network pharmacology and experimental validation

Ying Luo, Jing Xiang, Shuangyang Tang, Shiting Huang, Yishan Zhou, Haiyan Shen*

Institute of Biochemistry and Molecular Biology, The Key Laboratory of Environment and Critical Human Diseases Prevention of the Education Department of Hunan Province, Hengyang Medical College, University of South China, Hengyang 421001, China

ARTICLE INFO

Keywords:

Ursolic acid
Acute B lymphoblastic leukaemia
Apoptosis
Pyroptosis
JNK

ABSTRACT

Objective: To explore the mechanism of ursolic acid (UA) against acute B lymphoblastic leukaemia (B-ALL) based on network pharmacological analysis, molecular docking and experimental verification.

Methods: The core targets, functional processes, and biological pathways of UA in B-ALL were predicted by network pharmacology and molecular docking. The efficacy and mechanism of UA against B-ALL were verified through in vitro experiments such as cell viability assays, CCK-8 assays, LDH assays, AO/EB staining, flow cytometry, and Western blot assays.

Results: Network pharmacology analysis of the core targets indicated that the effects of UA on B-ALL were related to programmed cell death (apoptosis and pyroptosis). Molecular docking results showed that *FOS*, *CASP8*, *MAPK8*, *IL-1 β* and *JUN* were the key targets of UA against B-ALL. The MTS assay showed that UA decreased the viability of Reh cells in a concentration- and time-dependent manner. Cellular and Western blot experiments found that UA induced Reh cell apoptosis and pyroptosis by upregulating the JNK signalling pathway.

Conclusions: Our findings demonstrated that UA could induce Reh cell apoptosis and pyroptosis by activating the JNK signalling pathway to exert anti-B-ALL effects. This indicates that UA may become a potential drug for the effective treatment of B-ALL.

1. Introduction

Acute B lymphoblastic leukaemia (B-ALL) is recognized as the disease with the highest morbidity rate in acute lymphoblastic leukaemia and is caused by genetic variation and polymorphism of B-lineage lymphoid precursor cells and abnormal proliferation of leukaemia cells in the bone marrow [1,2]. At present, the clinical treatment of B-ALL is mainly based on chemotherapy; approximately 80 % of children and 30 % of adults have long-term survival as well as a chance of cure [3,4]. However, inducing a single form of programmed cell death (PCD), such as apoptosis, is prone to develop chemoresistance and results in leukaemia relapse [5]. At the same time, chemotherapy causes certain damage to normal cells. Therefore, finding natural compounds with low toxicity that can induce multiple types of PCD has become a new perspective to overcome leukaemia relapse, which is expected to solve the chemoresistance of

* Corresponding author.

E-mail address: 2015002076@usc.edu.cn (H. Shen).

<https://doi.org/10.1016/j.heliyon.2023.e23079>

Received 25 May 2023; Received in revised form 16 November 2023; Accepted 27 November 2023

Available online 1 December 2023

2405-8440/© 2023 Published by Elsevier Ltd.

This is an open access article under the CC BY-NC-ND license

(<http://creativecommons.org/licenses/by-nc-nd/4.0/>).

B-ALL treatment. In clinical treatment, traditional Chinese medicine is expected to be an alternative therapy or an adjunctive therapy for chemotherapy, due to its low toxicity and significant efficacy [6–8].

Ursolic acid (UA), a pentacyclic triterpenoid (Fig. 1), which is a major active component of the antitumour Chinese herbs *Cornus officinalis* and *Ligustrum lucidum* [9]. It has been reported that UA has strong inhibitory effects on a variety of tumours, including colon cancer, gastric cancer, liver cancer, breast cancer, and leukaemia [10,11]. UA exerts antitumour effects by inhibiting the cell cycle and proliferation, inducing differentiation and PCD, reversing drug resistance, and inhibiting invasion [12,13]. Therefore, UA is considered as one of the classic drugs for the treatment of tumours [14]. Previous studies have demonstrated that UA was able to inhibit the proliferation of the B-ALL cell line Reh [15]. However, the mechanism of action of UA against B-ALL is still unclear.

Thus, this study aimed to use network pharmacology and molecular docking to analyse the targets, biological functions, and signalling pathways of UA in B-ALL. Meanwhile, *in vitro* experiments with Reh cells exposed to UA were performed to further explore the mechanism of UA against B-ALL.

2. Materials and methods

2.1. Network pharmacology

The potential targets of UA were collected from the TCMSP database (<http://tcmspnw.com/>) and DrugBank database (<https://www.drugbank.ca/>). Additionally, the disease target information related to B-ALL was searched from web databases, including Genecards (<https://www.genecards.org/>) and OMIM (<https://omim.org/>). The targets of UA and B-ALL were analysed through the proportional Venn diagram in the bioinformatics database (<http://www.bioinformatics.com.cn/>) to obtain the overlapping gene targets. The intersecting targets between UA and B-ALL were imported into the STRING database (<https://string-db.org/>) and Cytoscape 3.7.2 software for protein–protein interaction (PPI) analysis. The Metascape database (<https://Metascape.org/gp/index.html>) was used for GO enrichment and KEGG pathway analysis. The whole *Homo sapiens* gene was chosen as the background gene dataset. A "UA-core targets-KEGG pathways-B-ALL" network diagram was constructed using Cytoscape 3.7.2 software (<http://www.cytoscape.org/>) and represented graphically.

2.2. Molecular docking

Molecular docking was used to further explore the possibility of drug regulation of key proteins in the signalling pathway of interest. The 3D crystal structure of the core target was downloaded from the RCSB PDB database (<https://www.rcsb.org/>), and AutoDock Vina 1.2.2 was used to evaluate the binding energy of the ligand and receptor. A binding energy ≤ 7.0 kcal/mol was considered to indicate strong binding ability [16]. PYMOL software was used to visualize the optimal binding mode.

2.3. *In vitro* experiments

2.3.1. Antibodies

Primary antibodies included anti-Caspase-8 (Proteintech, 13423-1-AP), anti-Bax (Proteintech, 50599-2-Ig), anti-Bcl-2 (26593-1-AP), anti-Caspase-1 (Arigo, ARG57293), anti-Cytochrome C (Cyt C) (Abcam, Ab133504), anti-Cleaved-Caspase-9 (Abcam, Ab2324), anti-Cleaved-PARP (Abcam, Ab32561), anti-NLRP3 (Abcam, Ab263899), anti-p-JNK (Abcam, Ab124956); anti-PARP (Beyotime Biotechnology, AF1657), anti-Caspase-3 (Beyotime Biotechnology, AF0081), anti-JNK (Beyotime Biotechnology, AF1048); anti-Cleaved-Caspase-3 (Cell Signaling Technology, 9664T); anti-IL-1 β (Arigo, ARG66285), anti-GSDMD (Arigo, A18281); and β -actin (Soiarbio, BL005B); secondary antibodies included HRP-conjugated Affinipure Goat Anti-Rabbit IgG (H + L) (Proteintech, SA00001-2) and HRP-conjugated Affinipure Goat Anti-Mouse IgG (H + L) (Proteintech, SA00001-1).

2.3.2. Cell culture

The human acute B lymphoblastic leukaemia cell line Reh and the human normal endothelial cell line HUVECs were obtained from the University of South China (Hengyang, China) and cultured in RPMI-1640 (Sigma–Aldrich, R8758) complete medium containing 10 % foetal bovine serum (ExCell Bio, FSP500) at 37 °C in a humidified incubator (Thermo Fisher Scientific) with 5 % CO₂.

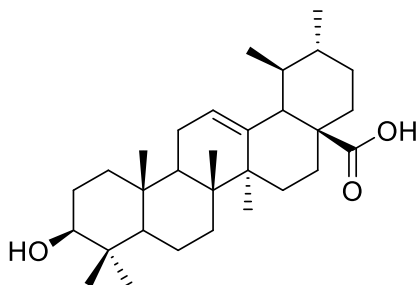


Fig. 1. Molecular structure of ursolic acid.

2.3.3. Cell viability assay and IC_{50} calculation

Reh and HUVEC cell proliferation was tested with CellTiter 96® Aqueous One Solution Cell Proliferation Assay (MTS) (Promega, G3580), and the half-maximal inhibitory concentration (IC_{50}) of UA (Macklin, U820363) on Reh cells was calculated by dose–response curve fitting. Briefly, Reh and HUVECs in log phase were cultivated in 96-well plates at a density of 1×10^4 cells/100 μ L. Then, Reh and HUVECs were exposed to different concentrations of UA (0, 10, 20, 30, 40 μ mol/L) for 12, 24 and 48 h. Next, 20 μ L MTS solution was added to each well and incubated in a CO₂ incubator for 3 h. Finally, the OD value was detected by an enzyme-linked immunosorbent (Bio-Tek) assay at 490 nm with a microplate reader (Bio-Rad, Hercules, USA). IC_{50} values were analysed by GraphPad Prism 8.

2.3.4. Cell proliferation assay

Cell viability assay was tested with a Cell Counting Kit-8 (CCK-8) assay (Dojindo, CK04). Reh cells were exposed to UA or the apoptosis-specific inhibitor Z-VAD-FMK (MedChemExpress, HY-16658B) for 24 h. Next, 10 μ L CCK-8 solution was added to each well and incubated in a CO₂ incubator for 3 h. Finally, the OD value was detected by an enzyme-linked immunosorbent assay at 450 nm. The formula for calculating cell viability is as follows:

$$\text{Inhibition rate (\%)} = \left(1 - \frac{\text{OD}_{\text{treated}} - \text{OD}_{\text{blank}}}{\text{OD}_{\text{control}} - \text{OD}_{\text{blank}}} \right) \times 100\%$$

2.3.5. LDH release assay

The LDH content in the culture medium was tested with an LDH Release Assay kit (Beyotime Biotechnology, C0016). Briefly, Reh cells were exposed to UA or Z-VAD-FMK at specific concentrations for 24 h. One hour before detection, 10 μ L of LDH release reagent was added to the designated wells. When the predetermined time was reached, the culture medium was collected at 1200 rpm/3 min. Sixty microlitres of culture medium and 30 μ L of LDH detection working solution (containing 10 μ L of lactic acid solution, 10 μ L of 1x INT solution and 10 μ L of enzyme solution) were added to the 96-well plate and incubated on a shaker for 30 min. The OD value was detected by an enzyme-linked immunosorbent assay at 490 nm.

2.3.6. Cell morphology assay

Reh cells in log phase were cultivated in 24-well plates at a density of 1×10^5 cells/100 μ L. Meanwhile, the cells were exposed to specific concentrations of UA for 24 h. Next, the changes in cell morphology were observed under an optical microscope (CX41; Olympus, Tokyo, Japan).

2.3.7. Cell membrane permeability assay

Cell membrane permeability was tested with acridine orange (AO)/ethidium bromide (EB) double fluorescence staining (Sangon Biotech, E607308-0100). Briefly, Reh cells were exposed to UA at specific concentrations. Next, the cells in each group were collected by centrifugation at 1200 rpm/3 min, washed twice with PBS, resuspended in 100 μ L staining solution (containing 90 μ L 1X Buffer, 5 μ L AO and 5 μ L EB), and incubated at room temperature for 5 min. After that, 25 μ L cell suspension was dropped onto a clean glass slide and covered with a coverslip. Finally, the fluorescence of the cells was observed and photographed by a fluorescence microscope, and the excitation light wavelength of blue light was 510 nm.

2.3.8. Mitochondrial membrane potential assay

Mitochondrial membrane potential (MMP) was tested with the JC-1 fluorescent probe (Beyotime Biotechnology, C2003S). Briefly, Reh cells were exposed to UA at specific concentrations. After that, cells in each group were collected by centrifugation at 1200 rpm/3 min, resuspended in 250 μ L staining solution (containing 248.5 μ L JC-1 staining buffer and 1.5 μ L 200x JC-1), and placed in a constant temperature incubator at 37 °C for 20 min. Next, the cells were centrifuged at 600 \times g for 4 min at 4 °C, washed twice with 1 mL of JC-1 staining buffer and resuspended. Finally, the cells were detected by flow cytometry (BD FACSCalibur), and the data were analysed with FlowJo 7.6.1 software.

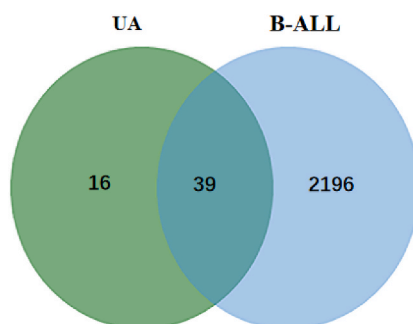


Fig. 2. Venn diagram of target gene intersections of UA- and B-ALL-related genes.

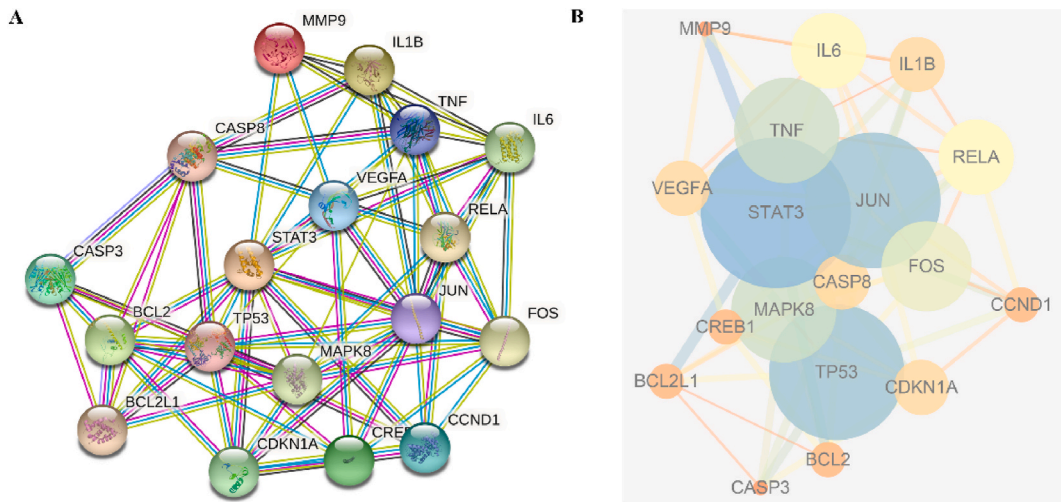


Fig. 3. The core targets of UA in B-ALL. (A) PPI network diagram of core targets. (B) Network analysis diagram of core targets.

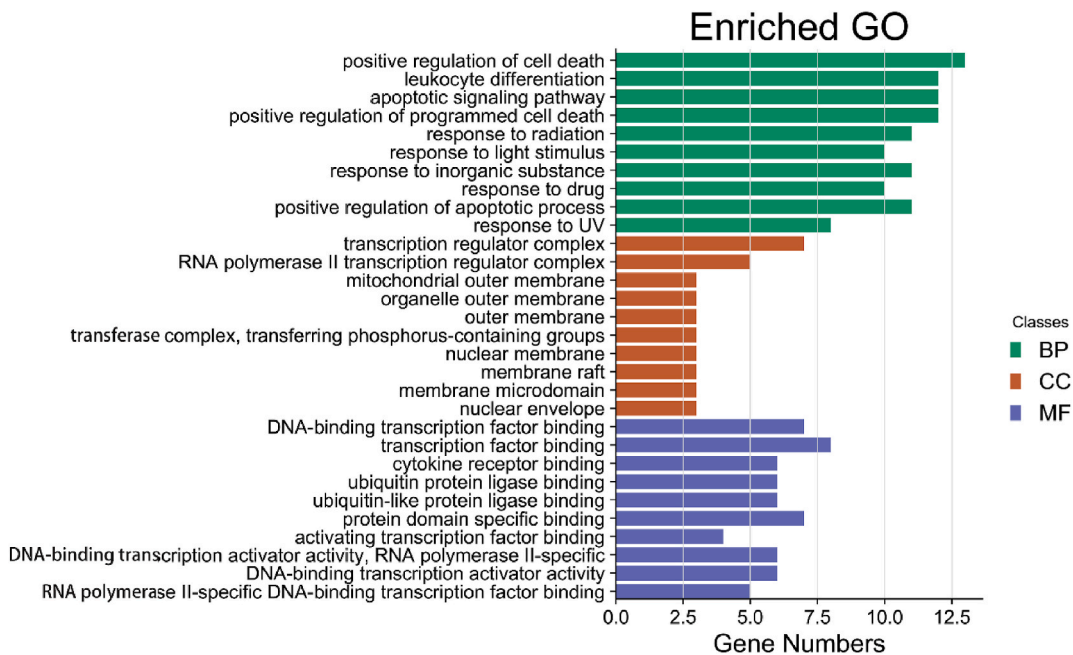


Fig. 4. GO enrichment analysis of core targets.

2.3.9. Apoptosis rate assay

The apoptosis rate was tested with an Annexin V-FITC/PI detection kit (KeyGEN BioTECH, KGA107). Briefly, Reh cells were exposed to UA or Z-VAD-FMK at specific concentrations. Then, the cells in each group were collected by centrifugation at 1200 rpm/3 min, washed twice with precooled PBS solution, resuspended in 500 μL staining solution (containing 490 μL binding buffer, 5 μL Annexin V-FITC and 5 μL PI), and incubated on ice for 5–15 min in the dark. Finally, the cells were detected by flow cytometry, and the data were analysed using FlowJo 7.6.1 software.

2.3.10. Western blot

Reh cells were exposed to UA, Z-VAD-FMK or SP600125 (MedChemExpress, HY-12041) for 24 h. Then, the cells in each group were collected by centrifugation at 1200 rpm/3 min, washed twice with precooled PBS solution and lysed with cell lysis buffer (containing 100 μL RIPA and 1 μL PMSF) (Solarbio, R0010) for approximately 30 min. Next, the protein solution was collected by cryogenic centrifugation at 13000 rpm/30 min, subjected to BCA (ComWin Biotech, CW0014) quantification, separated by 10%–15 % SDS–

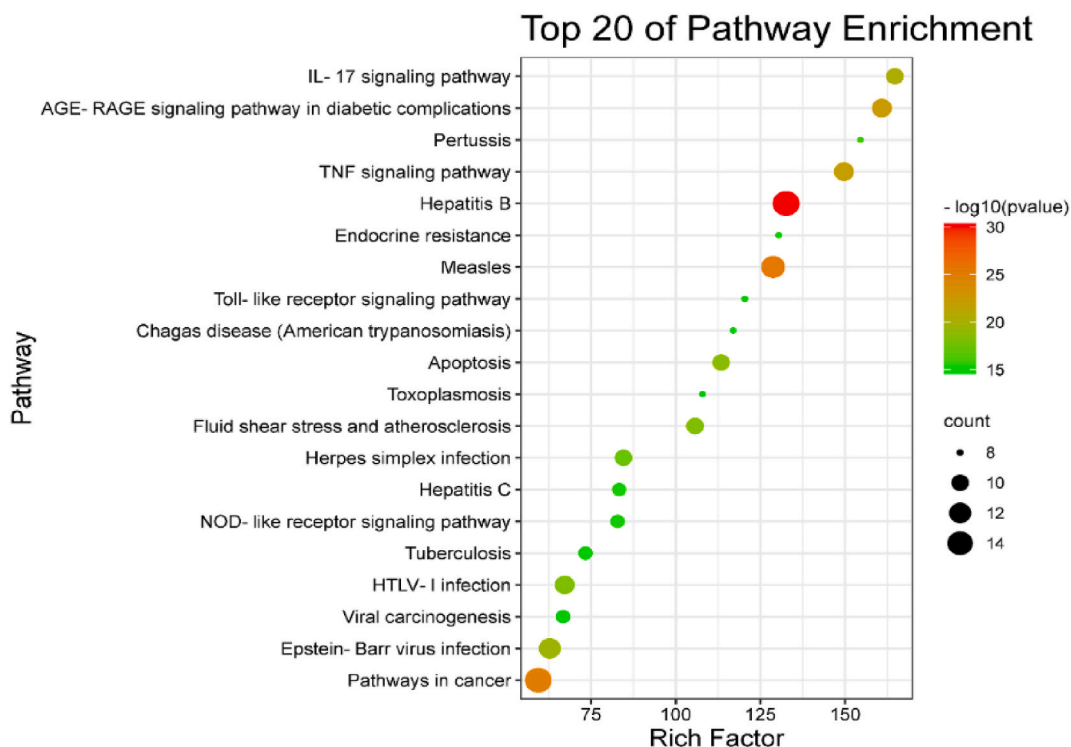


Fig. 5. KEGG enrichment analysis of core targets.

PAGE (Beyotime Biotechnology, P0012A) and transferred to a PVDF membrane (Millipore, IPVH00010). After that, the membrane was blocked in 5 % BSA (Solarbio, BL005B) at room temperature for 2 h, incubated with primary antibody overnight at 4 °C, washed 6 times with TBST, incubated with secondary antibody at room temperature for 1 h, and washed 6 times with TBST. Finally, ECL developer (New Cell & Molecular Biotech, P10100) was added dropwise, and the membrane was scanned and imaged using a chemiluminescence imager (Tanon).

2.4. Statistical analysis

Experimental data are expressed as the mean \pm standard deviation (SD) from triplicates of three independent experiments. Statistical analysis of experimental data by *t*-test or one-way analysis of variance (ANOVA) was performed using GraphPad Prism 8 software, and $P < 0.05$ was considered statistically significant.

3. Results

3.1. Results of network pharmacology

Network pharmacology analysis was performed to screen target proteins and enrich molecular pathways underlying ursolic acid's anti-B-ALL efficacy. In total, 55 proteins were identified as UA-related targets, 2235 B-ALL-associated genes were collected, and 39 overlapping genes were considered potential targets of UA against B-ALL (Fig. 2). Subsequently, a PPI network was constructed and analysed using the STRING11.0 database and Cytoscape3.7.2 software (Fig. 3A and B), which showed that 18 targets were obtained.

GO enrichment analysis also revealed that the regulation of the biological functions of PCD, mitochondria, transcription factors and cytokines was involved in the anti-B-ALL action of UA (Fig. 4). KEGG enriched signalling pathways were obtained, and the top 20 pathways were selected for mapping (Fig. 5). The results indicated that the targets were mainly concentrated in cancer, apoptosis and cytokine pathways. The "UA-core targets-KEGG pathways-B-ALL" network diagram is shown in Fig. 6, which had 40 nodes (1 compound, 18 targets, 20 KEGG pathways, and 1 disease) and 242 edges. The core targets obtained were MAPK8, RELA, JUN, TNF, CASP8, CASP3, IL6, FOS, BCL2, IL1B, and TP53 by topological analysis. Therefore, UA may exhibit anti-B-ALL effects through multiple signalling pathways.

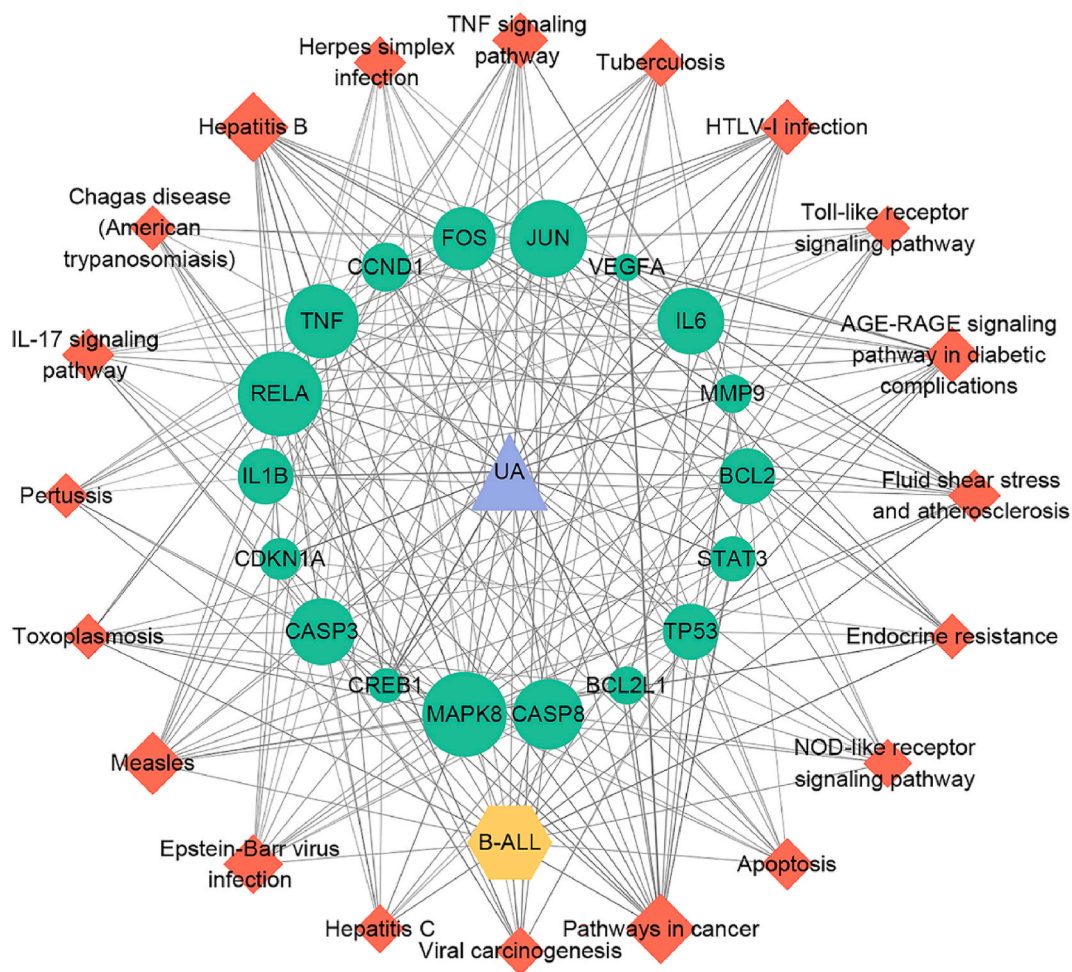


Fig. 6. The "UA-core targets-KEGG pathways-B-ALL" network diagram.

3.2. Results of molecular docking

Molecular docking was used to connect UA with the above core targets. In general, the lower the binding energy, the more stable the binding of the receptor to the ligand, and the easier it is to function. The binding energies of UA to core targets were all ≤ -7 kJ/mol, which indicated that UA had a strong affinity for these core targets. Among them, the docking results of *FOS*, *CASP8*, *MAPK8*, *IL1B* and *JUN* targets are shown in Fig. 7, which suggested that UA has the strongest affinity for *FOS* in the mitogen-activated protein kinase (MAPK) pathway.

3.3. In vitro experiments

3.3.1. The effect of UA on the viability of Reh and HUVECs

The effect of UA on the viability of the B-ALL cell line Reh and normal human umbilical vein endothelial cells (HUVECs) was tested by the MTS assay. The results showed that as the concentrations of UA increased and the treatment time of UA prolonged, the cell viability of Reh was progressively reduced compared with the that of 0 $\mu\text{mol/L}$ UA group (Fig. 8A), while the cell viability of HUVECs was not affected (Fig. 8B). Meanwhile, the IC_{50} values of UA in Reh cells were calculated to be 39.33, 32.01 and 26.22 $\mu\text{mol/L}$ at 12, 24 and 48 h, respectively (Fig. 8C). Therefore, UA inhibited the cell viability of Reh in a dose- and time-dependent manner.

3.3.2. The effect of UA on proliferation of Reh cells

Network pharmacology predicted that UA against B-ALL was associated with PCD (apoptosis and pyroptosis), so the morphological changes and inhibition ratio of Reh cells exposed to UA for 24 h were examined. The CCK-8 assays showed that the inhibition rate of Reh cells significantly increased with increasing concentrations of UA (Fig. 9A). Likewise, the number of Reh cells gradually decreased, and the abnormal cell morphology gradually increased. Among them, the 0 $\mu\text{mol/L}$ UA group had intact cell membranes and rounded

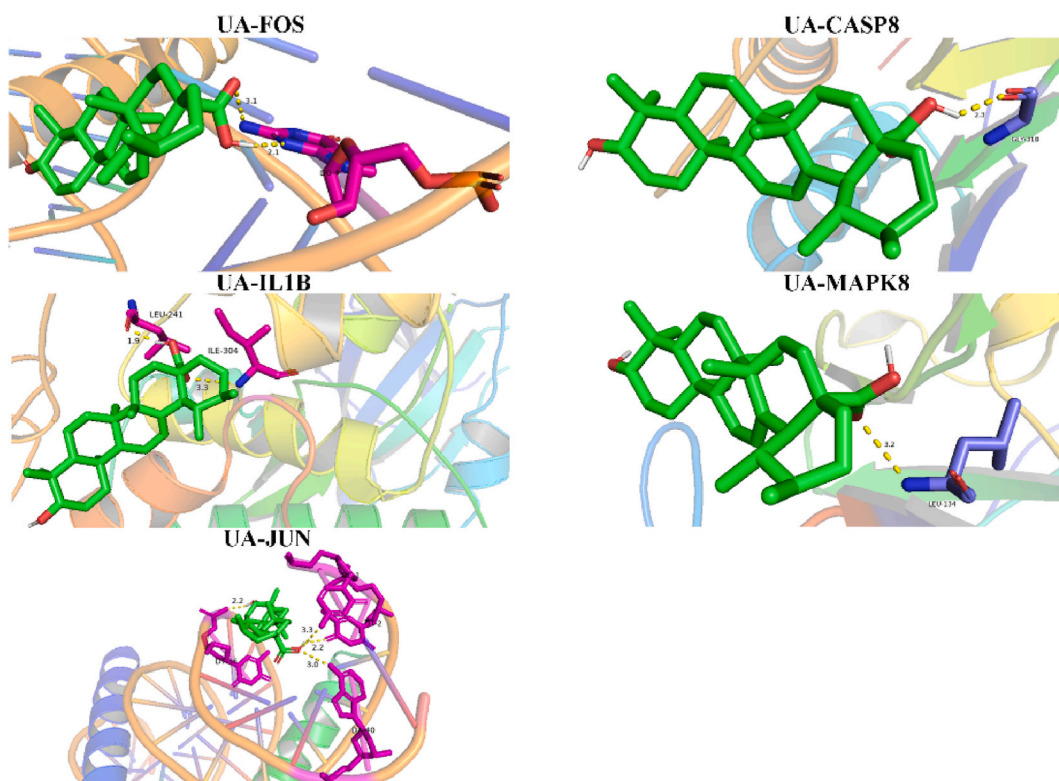


Fig. 7. Molecular docking models of UA and the top 5 core targets.

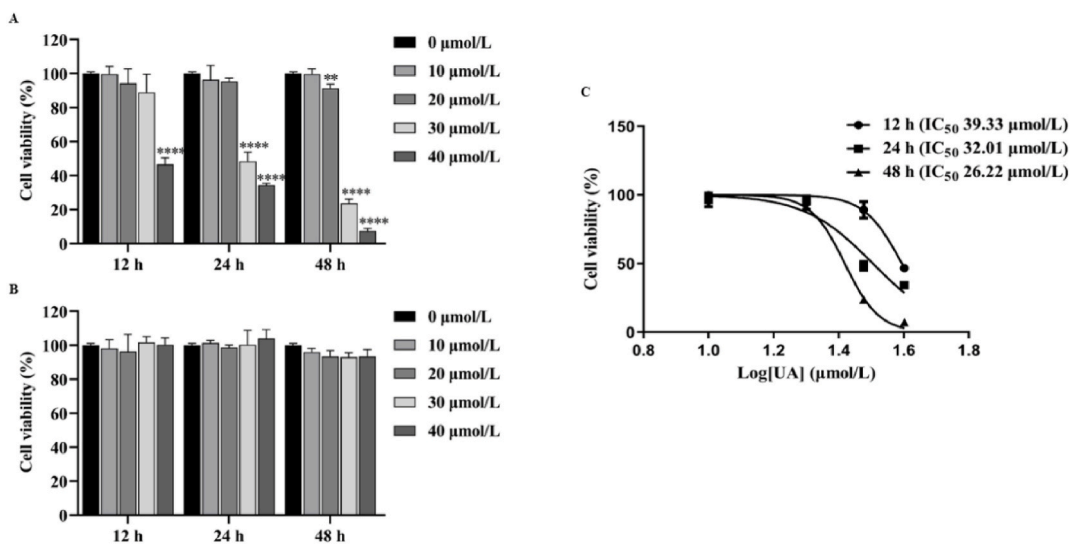


Fig. 8. Effects of different concentrations of UA on cell viability. (A) The effect of UA (0, 10, 20, 30 and 40 μmol/L) on the viability of Reh cells for 12 h, 24 h and 48 h. (B) The effect of UA (0, 10, 20, 30 and 40 μmol/L) on the viability of HUVECs for 12 h, 24 h and 48 h. (C) The IC₅₀ values of UA in Reh cells. Data are presented as the mean ± SD (n = 3). **P < 0.01, ****P < 0.0001 vs. 0 μmol/L UA.

cell morphology, while the 20, 30, and 40 μmol/L UA groups exhibited apoptotic morphology (cell shrinkage) and pyroptotic morphology (cell swelling) (Fig. 9B). The above results indicated that UA inhibited the proliferation of Reh cells. According to these experimental results, UA treatment at concentrations of 20, 30 and 40 μmol/L was selected for 24 h to carry out the subsequent experiments.

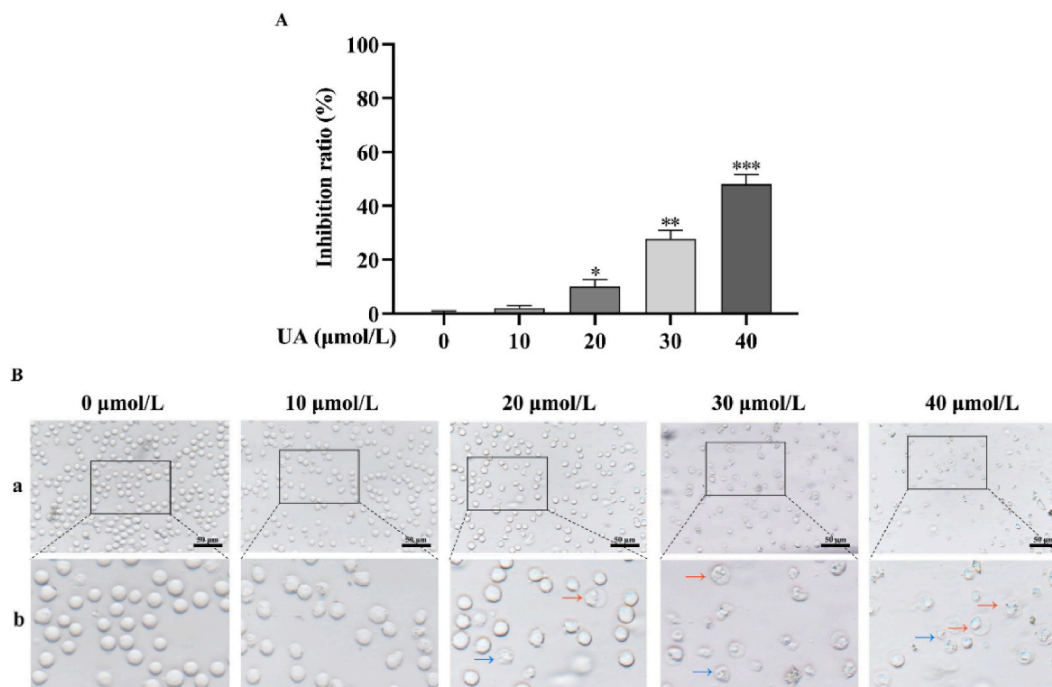


Fig. 9. The effect of UA on the proliferation of Reh cells. (A) The inhibition rate of Reh cells treated with UA was detected by CCK-8. (B) The effect of UA on the morphology of Reh cells (a: $\times 400$, b: partial enlargement; \rightarrow : cell shrinkage, \rightarrow : cell swelling). Data are presented as the mean \pm SD (n = 3). *P < 0.05, **P < 0.01, ***P < 0.001 vs. 0 $\mu\text{mol/L}$ UA.

3.3.3. The effect of UA on apoptosis of Reh cells

The KEGG pathway enrichment analysis predicted that UA against B-ALL was involved in the apoptosis signalling pathway. Meanwhile, the above experiments proved that UA-induced Reh cells exhibited apoptotic changes in morphology. Thus, the apoptosis-related indicators of Reh cells treated with UA were tested. First, the apoptosis rate in each group was detected by flow cytometry. Compared with the 0 $\mu\text{mol/L}$ UA group, the apoptosis rate gradually increased from $4.3 \pm 1.24\%$ to $4.8 \pm 1.62\%$, $14.5 \pm 4.08\%$ and $34.1 \pm 9.75\%$ (Fig. 10A and C). The results showed that UA induced a significant increase in the apoptosis rate of Reh cells. Then, the mitochondrial membrane potential (MMP) in each group was examined by JC-1 assay. When the concentration of UA was 40 $\mu\text{mol/L}$, the increase in green fluorescence and the decrease in red fluorescence were particularly remarkable (Fig. 10B and D). This result indicated that UA reduced the level of MMP in Reh cells. Finally, the expression of apoptosis-related proteins in each group was detected by Western blot assay. The results showed that with increasing concentrations of UA, the expression of cleaved caspase-8, cleaved caspase-9, cleaved caspase-3, cleaved PARP, the proapoptotic protein Bax and the MMP-related protein Cyt C was upregulated, while the expression of the antiapoptotic protein Bcl-2 was downregulated (Fig. 10E and F). In conclusion, UA induced Caspase-8-mediated mitochondrial apoptosis in Reh cells.

3.3.4. The effect of the apoptosis inhibitor Z-VAD-FMK on the proliferation of Reh cells inhibited by UA

The above experiments demonstrated that UA induced apoptosis in Reh cells. Therefore, the apoptosis-specific inhibitor Z-VAD-FMK was used to verify the results. The CCK-8 results showed that Z-VAD-FMK significantly enhanced the viability of UA-treated Reh cells (Fig. 11A). Furthermore, both flow cytometry and Western blot results showed that the apoptosis rate and the expression levels of the activated apoptotic proteins cleaved caspase-8 and cleaved caspase-3 in the Z-VAD-FMK + UA cotreatment group were significantly downregulated compared with those in the UA group (Fig. 11B–E). In addition, the LDH content in the culture medium of each group was also measured. The results showed that the LDH content of the Z-VAD-FMK + UA group was not significantly lower than that of the UA group (Fig. 11F). The above data suggested that Z-VAD-FMK reversed UA-inhibited proliferation in Reh cells by affecting apoptosis rather than pyroptosis.

3.3.5. The effect of UA on pyroptosis in Reh cells

Combining the predictions of network pharmacology and the experimental results of proliferation, the effect of UA on pyroptosis in Reh cells was investigated. The LDH assay showed that LDH release was significantly improved in the 30 and 40 $\mu\text{mol/L}$ UA groups compared with the 0 $\mu\text{mol/L}$ UA group (Fig. 12A). Meanwhile, the results of AO/EB staining showed that the Reh cells in the 0 $\mu\text{mol/L}$ UA group had normal morphology and green fluorescence, while the 20, 30, and 40 $\mu\text{mol/L}$ UA treatment groups had different degrees

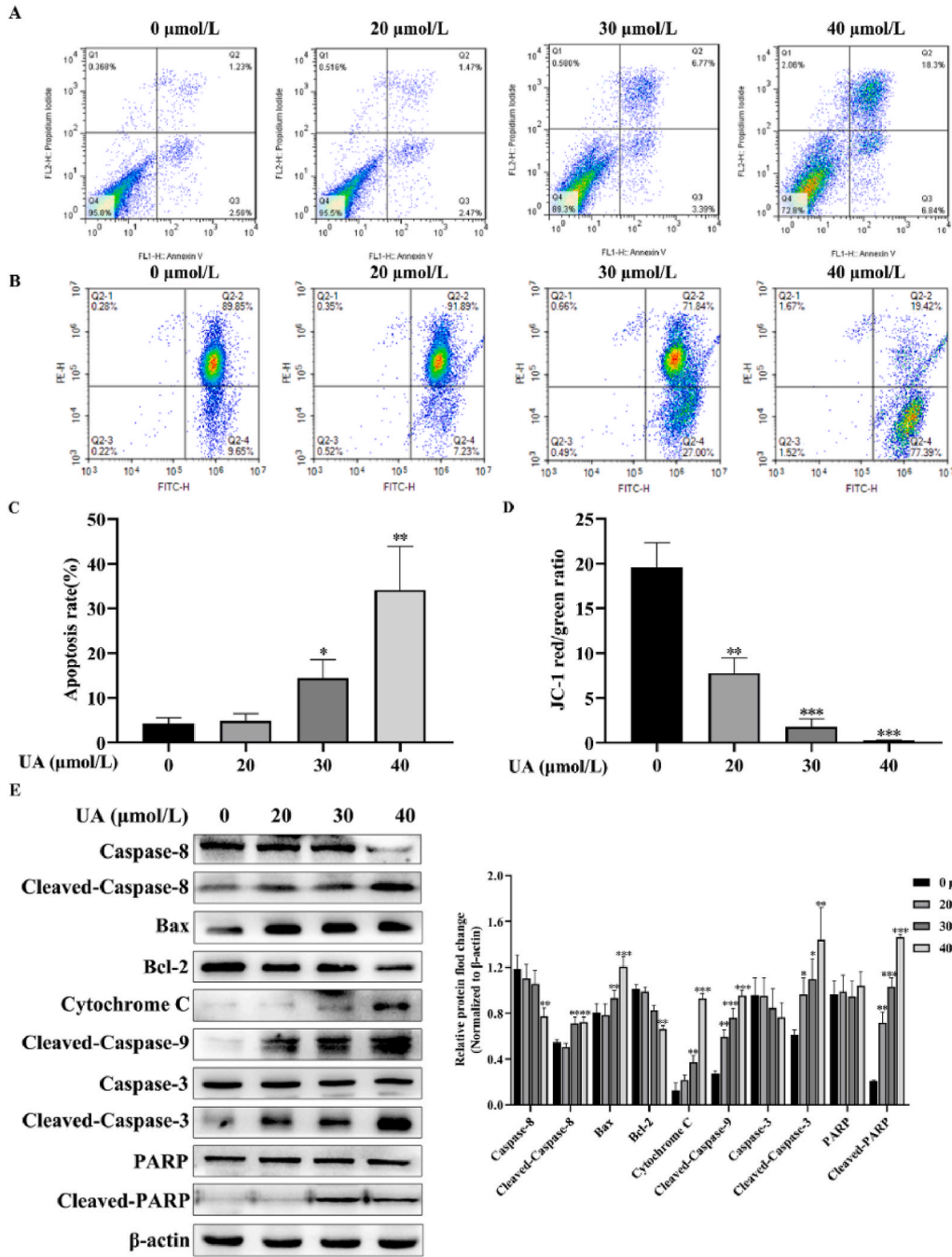


Fig. 10. The effect of UA on apoptosis in Reh cells. (A–D) The apoptosis rate and MMP of Reh cells exposed to UA were detected by flow cytometry. (E, F) The apoptosis proteins of Reh cells exposed to UA were detected by Western blot assays. Data are presented as the mean ± SD (n = 3). *P < 0.01, **P < 0.01, ***P < 0.001 vs. 0 μmol/L UA.

of red fluorescence, which showed a gradual increasing trend (Fig. 12B). The above experiments proved that UA improved the increase in LDH release and cell membrane permeability in Reh cells, indicating that Reh cells undergo pyroptosis. To verify that UA-induced pyroptosis in Reh cells is related to the Caspase-1-dependent pathway, the expression levels of pyroptotic proteins in each group were monitored by Western blot assay. The protein expression of NLRP3 and the ratio of Caspase-1/Pro-Caspase-1, Il-1β/Pro-Il-1β, and GSDMD-N/GSDMD-FL were markedly upregulated (Fig. 12C and D). In short, these results suggested that UA activated the Caspase-1-dependent pyroptotic pathway in Reh cells.

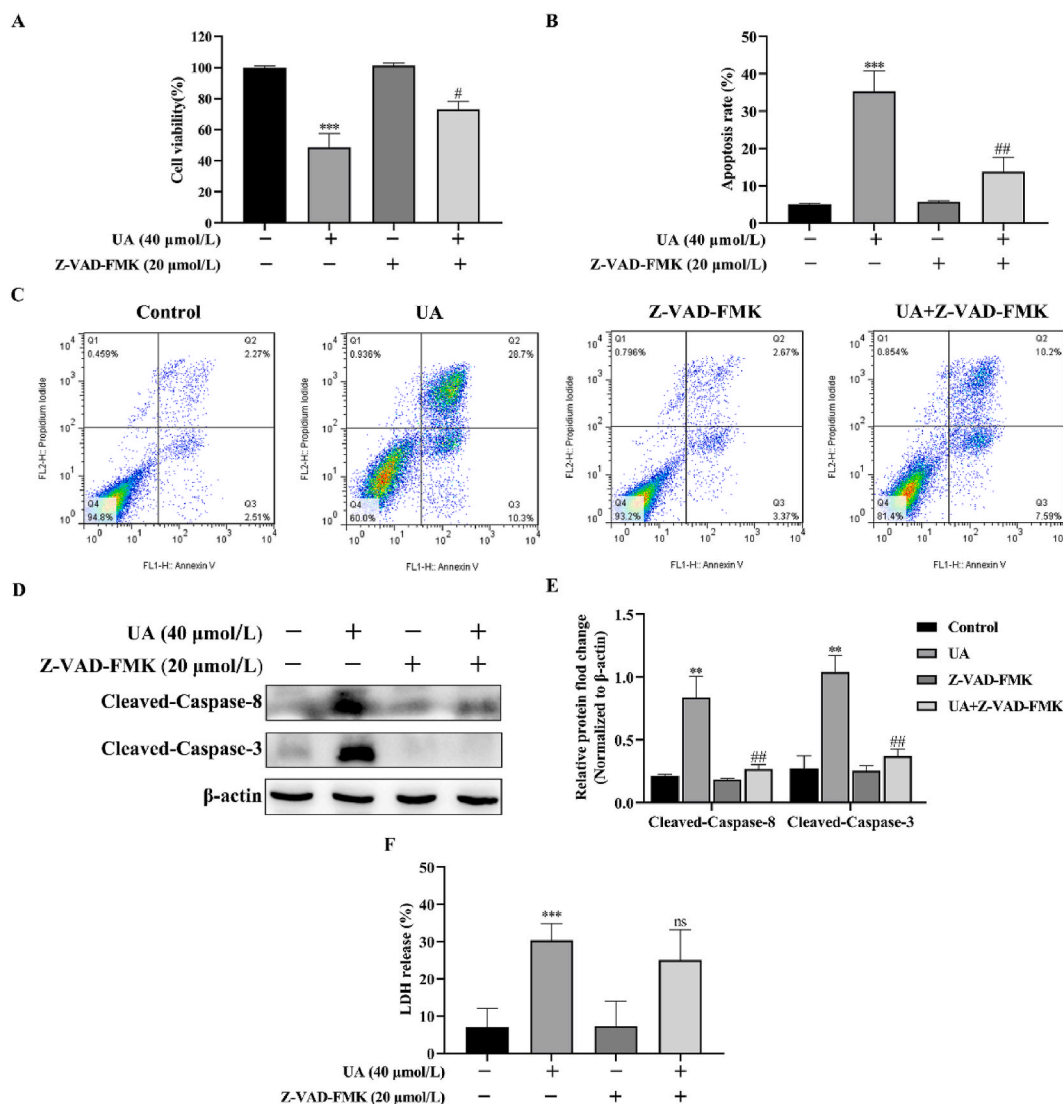


Fig. 11. The effect of Z-VAD-FMK on UA-induced proliferation in Reh cells. Reh cells were pretreated with 20 μmol/L Z-VAD-FMK, and then exposed to 40 μmol/L UA for 24 h. (A) The viability of Reh cells was detected by CCK-8. (B, C) The apoptosis rate of Reh cells was detected by flow cytometry. (D, E) The expression levels of cleaved caspase-8 and cleaved caspase-3 were detected by Western blot assays. (F) LDH release was detected by LDH assays. Data are presented as the mean ± SD (n = 3). *P < 0.05, **P < 0.01, ***P < 0.001 vs. Control; ns (not significant), #P < 0.05, ##P < 0.01 vs. 40 μmol/L UA.

3.3.6. UA suppressed the proliferation of Reh cells through the JNK signalling pathway

The results of network pharmacology and molecular docking suggested that the anti-B-ALL effect of UA was related to the JNK signalling pathway, so JNK signalling pathway related-proteins were assessed by Western blot assay. The results showed that the protein expression of p-JNK, p-c-Fos and p-c-Jun was gradually upregulated in Reh cells after treatment with 20, 30 and 40 μmol/L UA for 24 h, and the p-JNK/JNK ratio also increased (Fig. 13A and B). To further verify that the molecular mechanism of UA against B-ALL was correlated with the JNK signalling pathway, the JNK inhibitor SP600125 was used. Western blot analysis revealed that JNK signalling pathway proteins, including p-JNK, p-c-Fos and p-c-Jun, were downregulated in the SP600125+UA group compared with the UA group (Fig. 13C and D). The above results indicated that SP600125 could inhibit UA-activated expression of JNK signalling pathway proteins. Taken together, UA can suppress the proliferation of Reh cells by activating the JNK signalling pathway.

4. Discussion

According to the incidence data of leukaemia in China, ALL accounts for approximately 75 % of childhood leukaemia cases, and B-ALL ranks first. Due to the refractoriness and relapse of B-ALL, the prognosis of patients is still not optimistic. Therefore, it is necessary to find more effective and safer drugs and treatment methods. UA is a low-toxicity natural product that has obvious antitumour effects

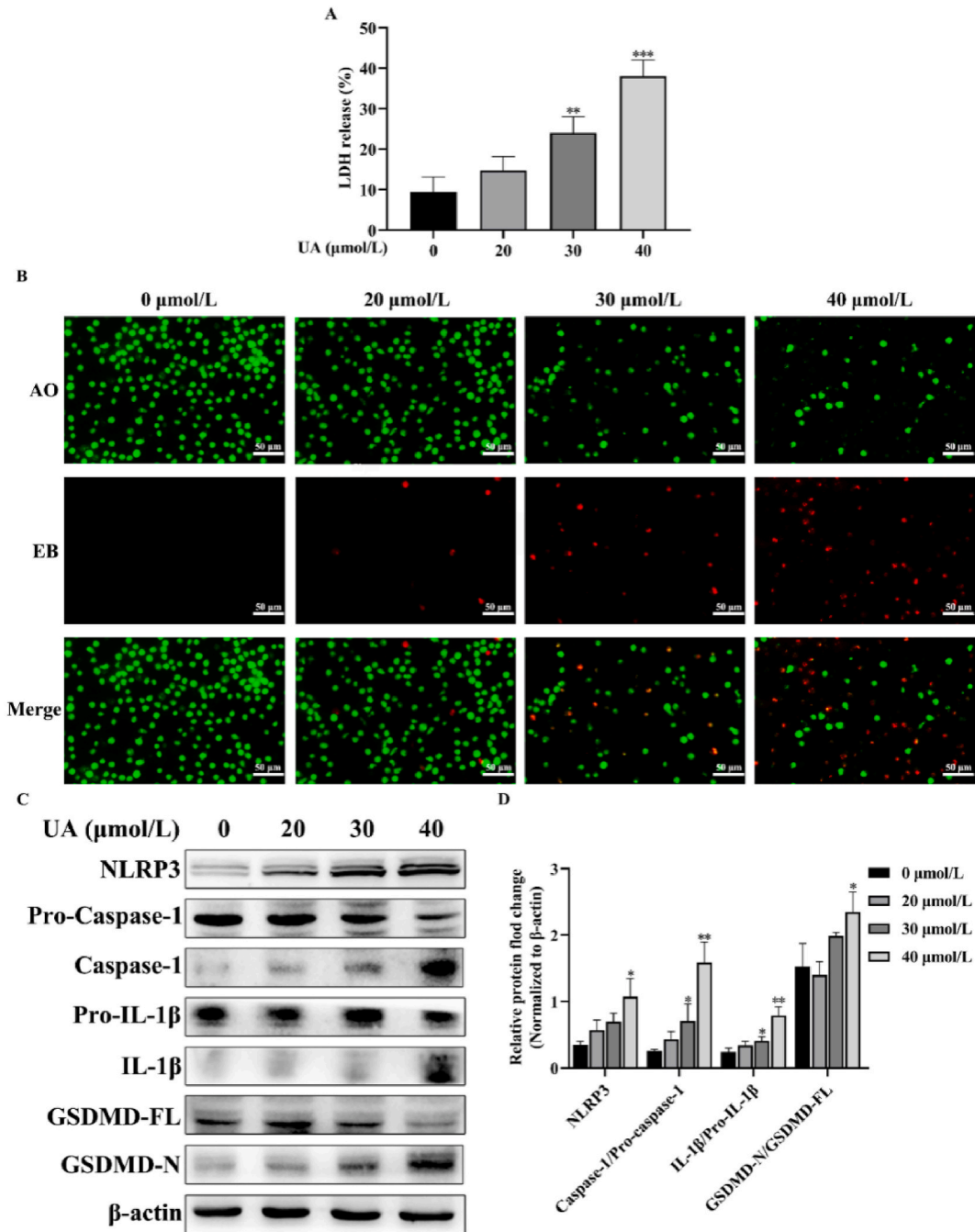


Fig. 12. The effect of UA on pyroptosis in Reh cells. (A) LDH release from Reh cells was examined by LDH assay. (B) The permeability of the Reh cell membrane was examined by AO/EB staining (× 400). (C, D) The pyroptosis proteins of Reh cells were examined by Western blot assays. Data are presented as the mean ± SD (n = 3). *P < 0.05, **P < 0.01, ***P < 0.001 vs. 0 μmol/L UA.

in various tumour cells [17]. Previous studies have demonstrated that UA can inhibit the proliferation of the B-ALL cell line Reh [15], but its underlying mechanism is unclear. The present study aimed to elucidate the mechanism of UA against B-ALL by network pharmacology, molecular docking and in vitro experimental validation.

Network pharmacology is a subject based on data analysis, database retrieval, and network construction. In recent years, network pharmacology has been widely used in the study of multiple targets and pathways of traditional Chinese medicine in the treatment of diseases [18]. In our study, network pharmacology and molecular docking analysis showed that UA mainly regulates *FOS*, *MAPK8*, *CASP8*, *IL-1β*, *JUN* and other targets, manipulates pathways in cancer, apoptosis and the NOD-like receptor pathway, and then affects cell proliferation, PCD, the mitochondrial outer membrane and other biological functions in B-ALL cells.

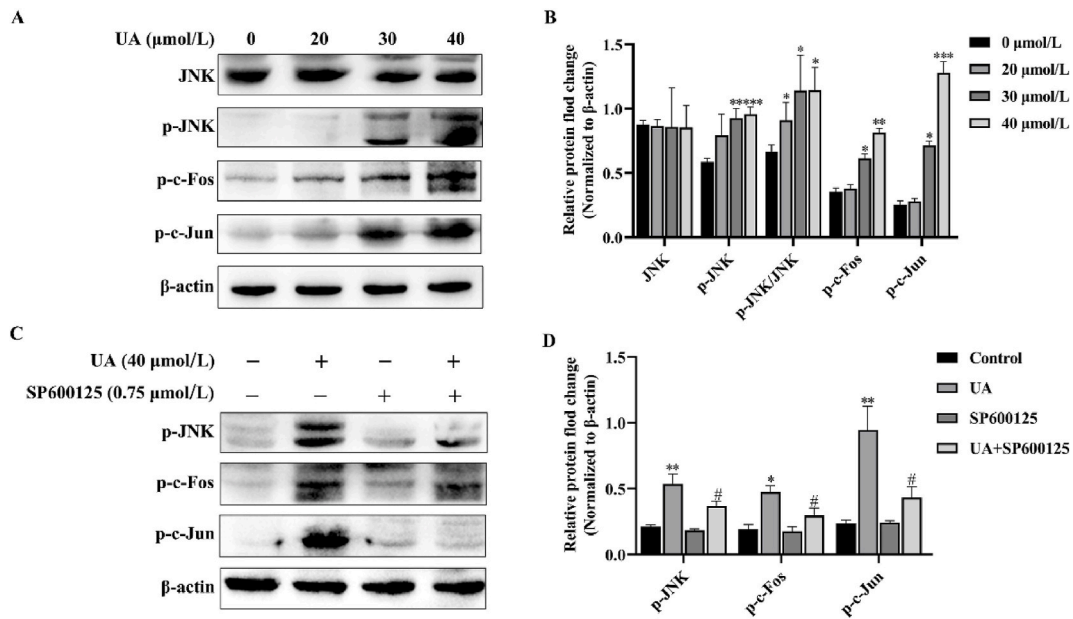


Fig. 13. UA activated the JNK signalling pathway in Reh cells. (A, B) The expression of JNK, p-JNK, p-c-Fos and p-c-Jun in Reh cells was monitored by Western blot assays. (C, D) Reh cells were pretreated with 0.75 μmol/L SP600125, and then exposed to 40 μmol/L UA for 24 h. The expression of p-JNK, p-c-Fos and p-c-Jun was monitored by Western blot assays. Data are presented as the mean ± SD (n = 3). *P < 0.05, **P < 0.01, ***P < 0.001 vs. 0 μmol/L UA; #P < 0.05, ##P < 0.01, ###P < 0.001 vs. 40 μmol/L UA.

PCD includes apoptosis, pyroptosis, etc., which plays a critical role in treating cancer [19]. It has been reported that UA initiates the apoptosis of leukaemia cells and inhibits tumour growth in mouse models [20]. In addition, activation of the NLRP3-mediated pyroptosis pathway can treat acute myeloid leukaemia [21,22]. However, PCD dysregulation is a major causative factor that results in the growth and drug resistance of many cancers [23]. Recent studies have revealed that inducing multiple types of PCD (apoptosis and pyroptosis) can reduce the drug resistance of cancer cells [24,25]. Our results found that UA inhibited the proliferation and induced abnormal morphology (shrinking and swelling) of Reh cells. Combined with the prediction results of network pharmacology, we speculated that UA might induce apoptosis and pyroptosis in Reh cells.

Cysteine aspartate protease 8 (Caspase-8), an initiator of apoptosis, can cleave Bid in the cytoplasm and trigger Bcl-2 family proteins, thereby activating the mitochondrial pathway [26,27]. The caspase-8-mediated mitochondrial pathway plays a significant role in inducing apoptosis of various cancer cells [28,29]. Our flow cytometry results demonstrated that UA induced mitochondrial damage in Reh cells and significantly increased the expression of the proteins Cyt C, cleaved caspase-3, cleaved caspase-8, cleaved caspase-9, and cleaved-PARP and the ratio of Bax/Bcl-2. Additionally, the apoptotic protein-specific inhibitor Z-VAD-FMK was used for reverse verification. The results showed that Z-VAD-FMK pretreatment improved cell viability, downregulated the expression of the cleavage proteins cleaved caspase-3 and cleaved caspase-8 and alleviated the UA-induced apoptosis rate. This indicated that Z-VAD-FMK can reverse the apoptosis of Reh cells induced by UA via the Caspase-8-mediated mitochondrial pathway.

Interleukin-1 beta (IL-1β) is involved in cytokine-mediated responses, and is located in the NLRP3/caspase-1-mediated classical pyroptosis pathway. In recent years, it was found that a variety of traditional Chinese medicines can induce tumour cell pyroptosis by NLRP3/caspase-1-mediated pathway [30–32]. In clinical studies, the prognosis of B-ALL was positively correlated with *CASP1* and *NLRP3* genes; that is, the high expression of *CASP1* and *NLRP3* genes indicated a good prognosis of B-ALL [33]. This result suggested that the pyroptosis has a strong correlation with the treatment and prognosis of B-ALL. Our results showed that UA induced LDH release and cell membrane damage in a concentration-dependent manner, and the expression of pyroptosis proteins (NLRP3, Caspase-1, IL-1β and GSDMD) was upregulated. Moreover, pretreatment with Z-VAD-FMK had no effect on UA-induced LDH release. In short, UA induced Caspase-1-dependent pyroptosis in Reh cells.

Mitogen-activated protein kinase 8 (MAPK8), namely, c-jun N-terminal kinase 1 (JNK1), is a member of the MAPK family. The transcription factors c-fos and c-Jun encoded by the *FOS* and *JUN* genes are downstream targets of JNK. In a variety of cancers, abnormally upregulated JNK protein controls various types of PCD, such as apoptosis, pyroptosis and autophagy [34,35]. In recent years, much evidence has demonstrated that activation of the JNK pathway is positively correlated with the antileukaemia effects [36–38]. Our Western blot results showed that the expression of p-JNK, p-c-Fos and p-c-Jun proteins was evidently upregulated; then, using SP600125 for reverse verification, it was found that SP600125 could downregulate the protein levels of p-JNK, p-c-Fos and p-c-Jun. This indicated that UA upregulated the JNK signalling pathway to inhibit apoptosis and pyroptosis in Reh cells.

5. Conclusions

In this study, combining network pharmacology, molecular docking and in vitro experiments, we confirmed that UA induced the apoptosis and pyroptosis of Reh cells through the upregulation of the JNK signalling pathway to exert anti-B-ALL effects. However, our present study is mainly based on in vitro cell experiments and is just a "first level study"; thus, in the future, in vivo animal experiments and further clinical studies should be devoted to evaluating the anti-B-ALL effects of UA. In conclusion, our study provides a new viewpoint for clarifying the mechanism of UA in the treatment of B-ALL.

Data availability statement

Data associated with our study has not been deposited into a publicly available repository. Data will be made available on request.

Ethical consent

No ethical consent was needed for this study.

Ethics statement

Review and/or approval by an ethics committee was not needed for this study because all study was done experimentally and no animal or human cases were recruited. Informed consent was not required for this study because no patient was recruited in this study.

CRediT authorship contribution statement

Ying Luo: Writing – original draft, Conceptualization. **Jing Xiang:** Project administration, Formal analysis. **Shuangyang Tang:** Writing – review & editing, Data curation. **Shiting Huang:** Resources, Methodology. **Yishan Zhou:** Resources, Methodology. **Haiyan Shen:** Writing – review & editing.

Declaration of competing interest

The authors declare that they have no known competing financial interests or personal relationships that could have appeared to influence the work reported in this paper.

Acknowledgments

This work was financially supported by the Science Fund of Hunan Provincial Education Department (20B504, 23B0395), the Natural Science Foundation of Hunan Province (2018JJ3433), the Planning Project for Science Research of Health and Family Planning Commission of Hunan Province (D202302047808), the Undergraduate Training Programs for Innovation and Entrepreneurship of Hunan Province (D202305162258543382), and the Undergraduate Training Programs for Innovation and Entrepreneurship of University of South China (2022X10555110).

Appendix B. Supplementary data

Supplementary data to this article can be found online at <https://doi.org/10.1016/j.heliyon.2023.e23079>.

References

- [1] M.B. Geyer, M. Hsu, S.M. Devlin, M.S. Tallman, D. Douer, J.H. Park, Overall survival among older US adults with ALL remains low despite modest improvement since 1980: SEER analysis, *Blood* 129 (13) (2017) 1878–1881.
- [2] T.C. Fujita, N. Sousa-Pereira, M.K. Amarante, M.A.E. Watanabe, Acute lymphoid leukemia etiopathogenesis, *Mol. Biol. Rep.* 48 (1) (2021) 817–822.
- [3] P. Brown, H. Inaba, C. Annesley, S. Colace, M. Dallas, K. DeSantes, K. Kelly, C. Kitko, N. Lacayo, N. Larrier, L. Maese, K. Mahadeo, R. Nanda, V. Nardi, V. Rodriguez, J. Rossoff, L. Schuettepelz, L. Silverman, J. Sun, W. Sun, D. Teachey, V. Wong, G. Yanik, A. Johnson-Chilla, N. Ogba, Pediatric acute lymphoblastic leukemia, version 2. 2020, NCCN clinical practice guidelines in oncology, *J. Natl. Compr. Canc. Netw.* 18 (1) (2020) 81–112.
- [4] F.L. Huang, E.C. Liao, C.L. Li, C.Y. Yen, S.J. Yu, Pathogenesis of pediatric B-cell acute lymphoblastic leukemia: molecular pathways and disease treatments, *Oncol. Lett.* 20 (1) (2020) 448–454.
- [5] D. Bhojwani, C.H. Pui, Relapsed childhood acute lymphoblastic leukaemia, *Lancet Oncol.* 14 (6) (2013) e205–e217.
- [6] K.Y. Tang, S.L. Du, Q.L. Wang, Y.F. Zhang, H.Y. Song, Traditional Chinese medicine targeting cancer stem cells as an alternative treatment for hepatocellular carcinoma, *J. Integr. Med.* 18 (3) (2020) 196–202.
- [7] X.Y. Zhang, H. Qiu, C.S. Li, P.P. Cai, F.H. Qi, The positive role of traditional Chinese medicine as an adjunctive therapy for cancer, *Biosci. Trends.* 15 (5) (2021) 283–298.
- [8] F.H. Qi, L. Zhao, A.Y. Zhou, B. Zhang, A.Y. Li, Z.X. Wang, J.Q. Han, The advantages of using traditional Chinese medicine as an adjunctive therapy in the whole course of cancer treatment instead of only terminal stage of cancer, *BioScience Trends* 9 (1) (2015) 16–34.
- [9] V. Khwaza, O.O. Oyediji, B.A. Aderibigbe, Ursolic acid-based derivatives as potential anti-cancer agents: an update, *Int. J. Mol. Sci.* 21 (16) (2020) 5920.

- [10] E.W.C. Chan, C.Y. Soon, J.B.L. Tan, S.K. Wong, Y.W. Hui, Ursolic acid: an overview on its cytotoxic activities against breast and colorectal cancer cells, *J. Integr. Med.* 17 (3) (2019) 155–160.
- [11] R. Yin, T. Li, J.X. Tian, P. Xi, R.H. Liu, Ursolic acid, a potential anticancer compound for breast cancer therapy, *Crit. Rev. Food Sci. Nutr.* 58 (4) (2018) 568–574.
- [12] L.L. Zang, B.N. Wu, Y. Lin, J. Wang, L. Fu, Z.Y. Tang, Research progress of ursolic acid's anti-tumor actions, *Chin. J. Integr. Med.* 20 (1) (2014) 72–79.
- [13] X.M. Feng, X.L. Su, Anticancer effect of ursolic acid via mitochondria-dependent pathways, *Oncol. Lett.* 17 (6) (2019) 4761–4767.
- [14] Y. Muto, M. Ninomiya, H. Fujiki, Present status of research on cancer chemoprevention in Japan, *Jpn. J. Clin. Oncol.* 20 (1990) 219–224.
- [15] Q. Ren, L.H. Sun, X.M. Liu, C.Y. Liu, L.H. Quan, C. Xie, Y.H. Liao, Active constituents from *Gardenia jasminoides* against acute lymphoblastic leukemia, *J. Guangdong Pharm. Coll.* 25 (2) (2009) 141–143.
- [16] F.A. Azri, J. Selamat, R. Sukor, N.A. Yusof, N.H.A. Raston, S. Eissa, M. Zourof, R. Chinnappan, Determination of minimal sequence for zearalenone aptamer by computational docking and application on an indirect competitive electrochemical aptasensor, *Anal. Bioanal. Chem.* 413 (15) (2021) 3861–3872.
- [17] W. Woessmann, M. Zimmermann, A. Meinhardt, S. Müller, H. Hauch, F. Knörr, I. Oeschles, W. Klapper, F. Niggli, E. Kabickova, A. Attarbaschi, A. Reiter, B. Burkhardt, Progressive or relapsed Burkitt lymphoma or leukemia in children and adolescents after BFM-type first-line therapy, *Blood* 135 (14) (2020) 1124–1132.
- [18] M. Alam, S. Ali, S. Ahmed, A.M. Elsbali, M. Adnan, A. Islam, M.I. Hassan, D.K. Yadav, Therapeutic potential of ursolic acid in cancer and diabetic neuropathy diseases, *Int. J. Mol. Sci.* 22 (2021), 12162.
- [19] J. Hitomi, D.E. Christofferson, A. Ng, J.H. Yao, A. Degterev, R.J. Xavier, J.Y. Yuan, Identification of a molecular signaling network that regulates a cellular necrotic cell death pathway, *Cell* 135 (7) (2018) 1311–1323.
- [20] G. Li, T. Zhou, L. Liu, J. Chen, Z. Zhao, Y. Peng, P. Li, N. Gao, Ezrin dephosphorylation/downregulation contributes to ursolic acid-mediated cell death in human leukemia cells, *Blood Cancer J.* 3 (4) (2013) e108.
- [21] W. Yang, S. Liu, Y.L. Li, Y.J. Wang, Y. Deng, W.M. Sun, H.L. Huang, J.M. Xie, A.D. He, H.L. Chen, A.L. Tao, J. Yan, Pyridoxine induces monocyte-macrophages death as specific treatment of acute myeloid leukemia, *Cancer Lett.* 492 (2020) 96–105.
- [22] D.C. Johnson, C.Y. Taabazuing, M.C. Okondo, A.J. Chui, S.D. Rao, F.C. Brown, C. Reed, E. Peguero, E. de Stanchina, A. Kentsis, D.A. Bachovchin, DPP8/DPP9 inhibitor-induced pyroptosis for treatment of acute myeloid leukemia, *Nat. Med.* 24 (8) (2018) 1151–1156.
- [23] E. Koren, Y. Fuchs, Modes of regulated cell death in cancer, *Cancer Discov.* 11 (2) (2021) 245–265.
- [24] L.F. Fu, A. Yonemura, N. Yasuda-Yoshihara, T. Umamoto, J. Zhang, T. Yasuda, T. Uchiyama, T. Akiyama, F. Kitamura, K. Yamashita, Y. Okamoto, L.K. Bu, F. Wei, X.C. Hu, Y. Liu, J.A. Ajani, P. Tan, H. Baba, T. Ishimoto, Intracellular MUC20 variant 2 maintains mitochondrial calcium homeostasis and enhances drug resistance in gastric cancer, *Gastric Cancer* 25 (3) (2022) 542–557.
- [25] J. Guo, J.B. Zheng, M.C. Mu, Z.L. Chen, Z.S. Xu, C.Y. Zhao, K. Yang, X. Qin, X.J. Sun, J.H. Yu, GW4064 enhances the chemosensitivity of colorectal cancer to oxaliplatin by inducing pyroptosis, *Biochem. Biophys. Res. Commun.* 548 (2021) 60–66.
- [26] X. Roucou, S. Montessuit, B. Antonssonet, J.C. Martinou, Bax oligomerization in mitochondrial membranes requires tBid (caspase-8-cleaved Bid) and a mitochondrial protein, *Biochem. J.* 368 (Pt 3) (2002) 915–921.
- [27] D.S. Simpson, J. Pang, A. Weir, L.Y. Kong, M. Fritsch, M. Rashidi, J.P. Cooney, K.C. Davidson, M. Speir, T.M. Djajawi, S. Hughes, L. Mackiewicz, M. Dayton, H. Anderton, M. Doerflinger, Y. Deng, A.S. Huang, S.A. Conos, H. Tye, S.H. Chow, A. Rahman, R.S. Norton, T. Naderer, S.E. Nicholson, G. Burgio, S.M. Man, J. R. Groom, M.J. Herold, E.D. Hawkins, K.E. Lawlor, A. Strasser, J. Silke, M. Pellegrini, H. Kashkar, R. Feltham, J.E. Vince, Interferon-gamma primes macrophages for pathogen ligand-induced killing via a caspase-8 and mitochondrial cell death pathway, *Immunity* 55 (3) (2022) 423–441.
- [28] J.H. Won, K.S. Chung, E.Y. Park, J.H. Lee, J.H. Choi, L.A. Taponjoui, H.J. Park, M. Nomura, A.H.E. Hassan, K.T. Lee, 23-hydroxyursolic acid isolated from the stem bark of *Cussonia bancoenis* induces apoptosis through fas/caspase-8-dependent pathway in HL-60 human promyelocytic leukemia cells, *Molecules* 23 (12) (2018) 3306.
- [29] K.H. Kim, H.S. Seo, H.S. Choi, I. Choi, Y.C. Shin, S.G. Ko, Induction of apoptotic cell death by ursolic acid through mitochondrial death pathway and extrinsic death receptor pathway in MDA-MB-231 cells, *Arch Pharm. Res. (Seoul)* 34 (8) (2011) 1363–1372.
- [30] J.F. Teng, Q.B. Mei, X.G. Zhou, Y. Tang, R. Xiong, W.Q. Qiu, R. Pan, B.Y. Law, V.K. Wong, C.L. Yu, H.A. Long, X.L. Xiao, F. Zhang, J.M. Wu, D.L. Qin, A.G. Wu, Polyphyllin VI induces caspase-1-mediated pyroptosis via the induction of ROS/NF-kappaB/NLRP3/GSDMD signal axis in non-small cell lung cancer, *Cancers* 12 (1) (2020) 193.
- [31] Z.Y. Cheng, Z.H. Li, L. Gu, L.Q. Li, Q. Gao, X.F. Zhang, J. Fu, Y.Y. Guo, Q.R. Li, X. Shen, M.J. Chen, X. Zhang, Ophiopogonin B alleviates cisplatin resistance of lung cancer cells by inducing caspase-1/GSDMD dependent pyroptosis, *J. Cancer* 13 (2) (2022) 715–727.
- [32] Y.M. Chen, B.X. Tang, W.Y. Chen, M.S. Zhao, Ursolic acid inhibits the invasiveness of A498 cells via NLRP3 inflammasome activation, *Oncol. Lett.* 20 (5) (2020) 170.
- [33] J. Singh, S. Kumari, M. Arora, D. Verma, J.K. Palanichamy, R. Kumar, G. Sharma, S. Bakhshi, D. Pushpam, M.S. Ali, A. Ranjan, P. Tanwar, S.S. Chauhan, A. Singh, A. Chopra, Prognostic relevance of expression of EMP1, CASP1, and NLRP3 genes in pediatric B-lineage acute lymphoblastic leukemia, *Front. Oncol.* 11 (2021), 606370.
- [34] B. Li, P.T. Zhou, K.H. Xu, T.R. Chen, J. Jiao, H.F. Wei, X.H. Yang, W. Xu, W. Wan, J.R. Xiao, Metformin induces cell cycle arrest, apoptosis and autophagy through ROS/JNK signaling pathway in human osteosarcoma, *Int. J. Biol. Sci.* 16 (1) (2020) 74–84.
- [35] Q.Y. Ding, W.D. Zhang, C. Cheng, F.B. Mo, L. Chen, G.F. Peng, X.Y. Cai, J.L. Wang, S.H. Yang, X.Z. Liu, Dioscin inhibits the growth of human osteosarcoma by inducing G2/M-phase arrest, apoptosis, and GSDME-dependent cell death in vitro and in vivo, *J. Cell. Physiol.* 235 (5) (2020) 2911–2924.
- [36] M.M. Mc Gee, G. Campiani, A. Ramunno, V. Nacci, M. Lawler, D.C. Williams, D.M. Zisterer, Activation of the c-Jun N-terminal kinase (JNK) signaling pathway is essential during PBOX-6-induced apoptosis in chronic myelogenous leukemia (CML) cells, *J. Biol. Chem.* 277 (21) (2002) 18383–18389.
- [37] N. Sabatini, V. Di Giacomo, M. Rapino, R. Rana, G. Garaci, A. Cataldi, JNK/p53 mediated cell death response in K562 exposed to etoposide-ionizing radiation combined treatment, *J. Cell. Biochem.* 95 (3) (2005) 611–619.
- [38] X.S. Liu, J. Jiang, Induction of apoptosis and regulation of the MAPK pathway by ursolic acid in human leukemia K562 cells, *Planta Med.* 73 (11) (2007) 1192–1194.